KPF: Keck Planet Finder

Steven R. Gibson[a], Andrew W. Howard[b], Geoffrey W. Marcy[a], Jerry Edelstein[a], Edward H. Wishnow[a], and Claire L. Poppett[a]

[a]Space Sciences Laboratory, University of California, Berkeley, United States
[b]Institute for Astronomy, University of Hawai'i, Honolulu, United States

ABSTRACT

KPF is a fiber-fed, high-resolution, high-stability spectrometer in development at the UC Berkeley Space Sciences Laboratory for the W.M. Keck Observatory. The instrument is designed to characterize exoplanets via Doppler spectroscopy with a single measurement precision of $0.5\,\mathrm{m\,s^{-1}}$ or better, however its resolution and stability will enable a wide variety of astrophysical pursuits. KPF will have a 200 mm collimated beam diameter and a resolving power of $>80{,}000$. The design includes a green channel (440 nm to 590 nm) and red channel (590 nm to 850 nm). A novel design aspect of KPF is the use of a Zerodur optical bench, and Zerodur optics with integral mounts, to provide stability against thermal expansion and contraction effects.

Keywords: Spectrometer, exoplanets, Doppler spectroscopy, Zerodur

1. INTRODUCTION

KPF is a fiber-fed, high-resolution, high-stability spectrometer in development at the Space Sciences Laboratory (SSL) of the University of California, Berkeley, for the W.M. Keck Observatory (WMKO)*. The instrument is designed to characterize exoplanets via Doppler spectroscopy with a single measurement precision of $0.5\,\mathrm{m\,s^{-1}}$ or better, however, its resolution and stability will enable a wide variety of astrophysical pursuits. KPF will cover a wavelength range of 440 nm to 850 nm over green and red channels.

The project has successfully passed the WMKO Science and Capabilities Review, as well as the System Design Review (equivalent to a Conceptual Design Review), and has attained the status of an official WMKO facility instrument. The project is currently within the preliminary design phase, with first light expected in mid-2019.

The initial baseline for the instrument included a green channel only, with the red channel as a future addition. At the recommendation of the WMKO Science Steering Committee, the red channel has recently been included into the baseline design.

2. SCIENCE CASE

KPF will be a broadly capable high-resolution optical spectrometer. Its primary science driver is to measure the masses and orbital properties of Earths, super-Earths, and sub-Neptunes that are known to be common from Doppler surveys[1–3] and the Kepler mission.[4] KPF will measure precise stellar Doppler shifts due to the gravitational pull of orbiting planets. KPF will be used to discover planets, particularly around nearby, bright stars and will excel at measuring the masses of planets discovered by transiting programs such as Kepler, TESS, and PLATO.

KPF will be particularly effective for transiting planet follow-up because of the Doppler precision (requirement: $0.5\,\mathrm{m\,s^{-1}}$ systematic error floor) and the large diameter of the 10 m Keck II telescope. These two requirements, minimizing errors in Doppler shifts caused by instrumental effects, and maximizing optical throughput, drive the KPF design. In the expected discovery space for TESS (Figure 1), KPF will measure planet masses for stars as faint as ∼15th magnitude, while similar precision instruments on 3 m class instruments will struggle to

Corresponding author email: sgibson@ssl.berkeley.edu

*During the conceptual development phase, the instrument was known as SHREK (Stable High Resolution Echelle for Keck).

Ground-based and Airborne Instrumentation for Astronomy VI, edited by Christopher J. Evans, Luc Simard, Hideki Takami
Proc. of SPIE Vol. 9908, 990870 · © 2016 SPIE · CCC code: 0277-786X/16/$18 · doi: 10.1117/12.2233334

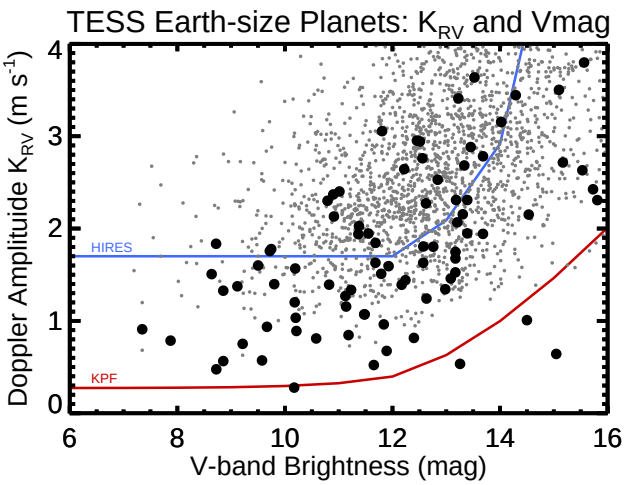

Figure 1. Expected planet discovery space for NASA's TESS mission with estimated sensitivity curves for KPF and HIRES at Keck Observatory. Super-Earth planets (R_p = 1.5–4 $R_\oplus$) are denoted by gray points, while Earth-size planets (R_p = 0.75–1.5 $R_\oplus$) are shown as black points. The planet sample is from a simulation of the TESS mission[5] and a mass-radius relationship. Only main sequence G, K, and early M type stars ($R_\star < 1.5\,R_\odot$ and $T_{\rm eff}$ = 3200–6200 K) are shown.

reach fainter than magnitude 12.5. Thus, KPF will be able to measure the masses of hundreds of TESS-discovered planets to map out the diversity of planet masses and densities (a clue to composition) in the Earth-to-Neptune regime. KPF will also be able to measure the mass function of Earth-size planets from Kepler to determine if these planets are commonly rocky or are enveloped in thick, low-density envelopes.

For nearby stars, KPF will catalog the planets in the solar neighborhood and will provide targets for planet imaging by WFIRST and giant segmented mirror telescopes (GSMTs; 30 m class). Planets orbiting early M dwarfs are particularly compelling because Earth-mass planets in the traditionally-defined Habitable Zone are detectable with KPF and these planets are also imageable by GSMTs.

Additional science cases for KPF stem from its general use as a high-resolution optical spectrometer and its high stability. These include stellar characterization (particularly to follow up transiting planet missions), exoplanet atmosphere spectroscopy, detection of the expansion of the universe in real time with Lyman-α forest spectroscopy, galactic chemical abundance archeology, spectroscopy of solar system objects, and isotopic abundance measurements from precise line shapes.

3. SYSTEM OVERVIEW

The KPF instrument will be comprised of several subsystems, each of which is described within this section. An overview of the KPF system is shown in Figure 2.

3.1 Fiber Injection Unit

Light from the Keck II telescope will feed the KPF Fiber Injection Unit (FIU), which will be located on the Nasmyth platform of the Keck II telescope. This system will include an atmospheric dispersion corrector (ADC), a tip/tilt mirror for image stabilization, a calibration light input, and the WMKO-standard MAGIQ[6] acquisition and guide camera. The FIU also focuses light from the telescope onto a science fiber, a sky fiber (located a few arcseconds away from the science fiber, to monitor contamination from moonlight and the sky background), and a fiber sending UV light to a small spectrometer monitoring the Calcium H & K spectral lines (to monitor magnetic activity that affects Doppler shifts).

The FIU will be designed, assembled and tested by WMKO for the KPF project. This is an ideal arrangement, as the FIU will have several direct interfaces with existing WMKO infrastructure, including the telescope itself and the guide camera feedback and control software.

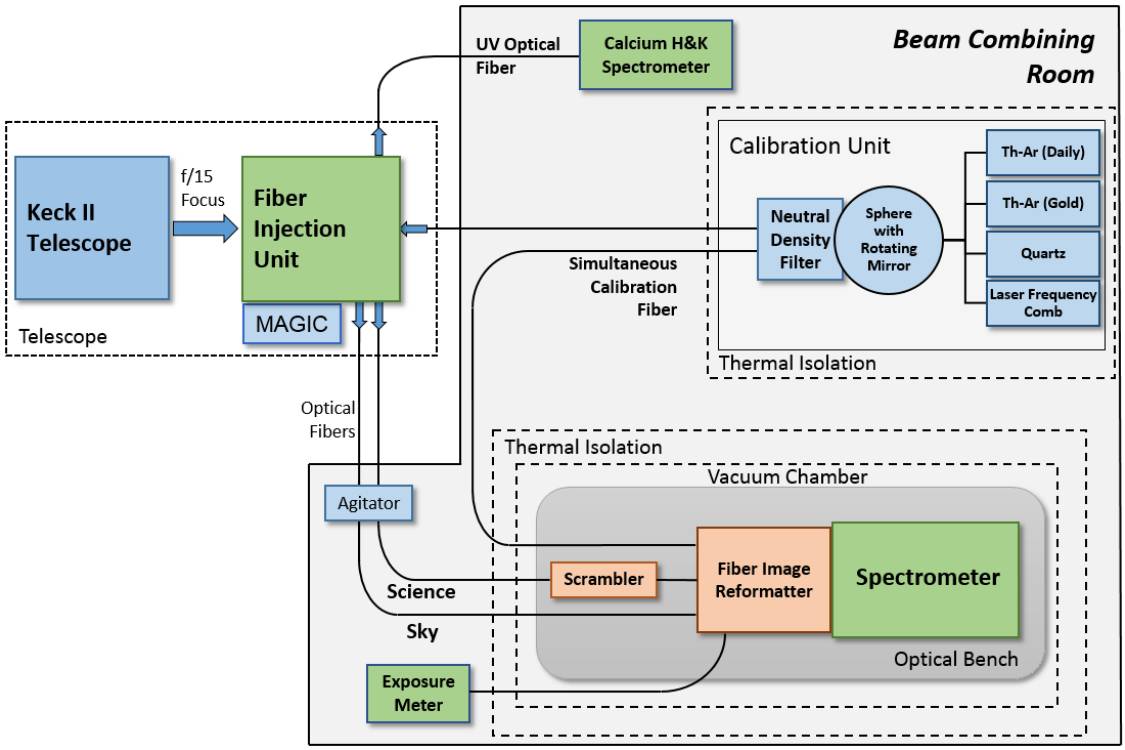

Figure 2. Schematic overview of the KPF system. The spectrometer and auxiliary subsystems will be located within the observatory basement, within the "beam combining room" (named for its purpose with the Keck Interferometer).

3.2 Illumination Homogenization System

The science and sky fibers will travel 70 m to the KPF spectrometer, located in the observatory basement. This length of fiber is required to negotiate the telescope structure, travel though the azimuth cable wrap, and then travel under the dome floor to the observatory basement. Long fiber runs suffer from preferential blue absorption, and over the green channel the flux at the blue end is 21% less than at the red end (considering only the internal transmission of the fiber). As a potential way to shorten our long fiber run, we investigated using the existing Keck Interferometer coudé train, but due to the extra optics involved found the efficiency gains to be minimal, and the potential observatory operations impact to be much higher, compared to the long fiber run.

Stable illumination of the spectrometer is paramount as any changes of the light distribution in either the image or pupil planes can cause displacements of the spectrum that nearly mimic Doppler shifts. An optical fiber feed is well known to serve as a "scrambler", transforming illumination changes at the input to the fiber (at the telescope focal plane) to a more homogeneous output that illuminates of the spectrometer.[7] To improve the scrambling performance, the science fiber will be an octagonal fiber,[8,9] and the fiber system will include additional scrambling,[10] consisting either of a small ball lens[11] or a pair of achromatic lenses,[12] that swap the near and far fields of the fiber output. The scrambler then feeds a short, 5 m length of octagonal fiber to further homogenize the scrambler output. Fiber modal noise can also cause illumination instabilities at the output of a fiber,[13,14] and to mitigate this effect an agitator[15] will be employed to mechanically wiggle the science and sky fibers. Our team has been testing fibers in our laboratory at SSL, with recent results presented elsewhere in these proceedings (Reference 16).

3.3 Reformatter

Following the scrambler, the science fiber ends at the input to the reformatter. This system (Figure 3) takes the light leaving the science fiber, and rearranges it into three "slices", aligned along the spectrometer (virtual) slit. This system effectively allows the KPF spectrometer to be three times smaller than a traditional spectrometer would be, given the aperture and image scale of the Keck telescopes. It allows a large fiber to be used at the

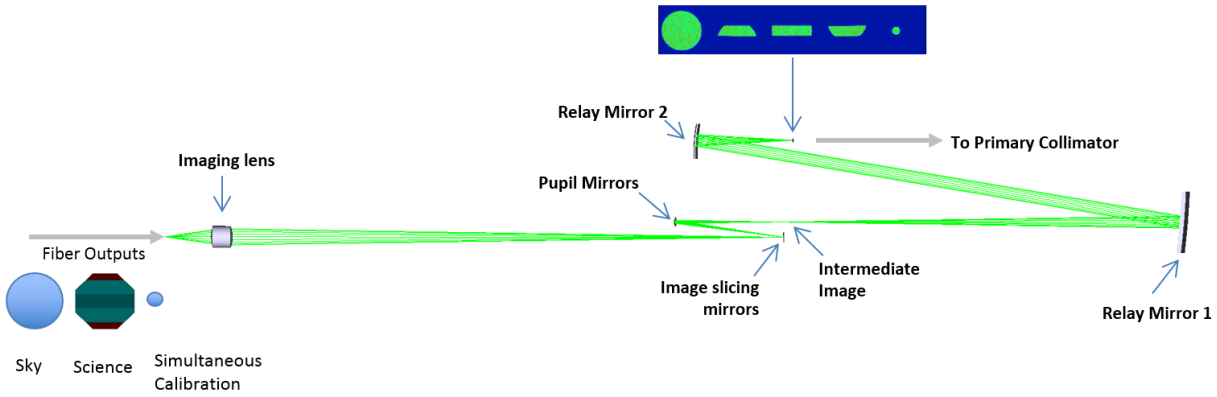

Figure 3. Optical design of the KPF reformatter. The inset shows the image presented at the spectrometer slit location, with the science fiber sliced three times and the shape of the calibration and sky fiber outputs unchanged.

telescope focal plane (to collect starlight), while presenting the spectrometer with a narrow "slit width" (which allows high resolution).

Light from the sky, science, and simultaneous calibration fiber is incident on the reformatter, as shown at the left of Figure 3. A triplet lens magnifies the fiber outputs by a factor of ten, and forms an image of them on the image slicing mirrors. The science fiber image falls on three slicing mirrors, which then redirect the separate slices towards the pupil mirrors, which refocus the light to an intermediate image. The sky and simultaneous calibration fiber images are not sliced, but rather fall on separate mirrors on either side of the slicing and pupil mirrors, and also reach focus at the intermediate image. This intermediate image is then demagnified by a pair of relay mirrors, to form an f/8 image at the slit position of the spectrometer.

The optical design of the reformatter is based on that shown in Reference 17. After some in-house KPF-specific modifications to the design, Winlight Systems was engaged to develop the optimized design shown in Figure 3. The KPF reformatter will be fabricated by Winlight Systems, with the reformatter mirrors optically contacted to a Zerodur base for high mechanical stability.[18]

Within Figure 3, the three green bands on the face of the science fiber represent the science slices accepted by KPF. Our science fiber size (250 μm) was determined through a trade study investigating Mauna Kea mean seeing conditions, fiber input f/ratio, number of slices, and bandpass for a given detector. In the chosen scheme, the outboard slices are narrower than the core science slices, and are of a more trapezoidal shape. As such, these outboard slices were rejected from the science spectrum, as their resolution elements would be quite different than the core science slices, and would also cost detector space (bandpass). Although the light path is not shown in Figure 3, the smaller outboard slices will utilized by an exposure meter system (described below).

An important point to note is that the reformatter is presented with a uniformly illuminated source to be sliced, as it is fed by the output of the entire illumination homogenization system (Figure 4). This is a very different situation than placing a traditional slicer at the focal plane of a telescope, where the illumination stability suffers from seeing and guiding issues. By placing the reformatter after the homogenization system, the intent is to minimize the changes in illumination between each slice. This is an important stability concern, and the illumination stability of our entire fiber, scrambler, and reformatter system will be confirmed by laboratory tests during the preliminary design phase.

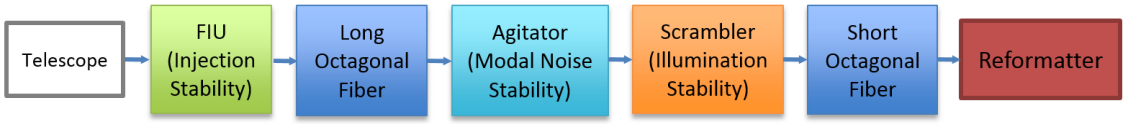

Figure 4. Components of the KPF illumination homogenization system.

We intend to treat each science slice independently during reduction. Due to alignment tolerances during the fabrication of the reformatter, we expect unavoidable offsets in the wavelength solution between slices, and therefore will not simply collapse the three slices together, but rather treat each as an independent measurement during reduction. We are also analyzing the effect of cross-talk between the slices, to ensure that it does not compromise our measurement precision.

3.4 Spectrometer Optical Design

The KPF spectrometer is of a white pupil optical design, the format of choice for existing (HARPS,[19] HARPS-N[20]) and planned (CARMENES,[21] ESPRESSO,[22] G-CLEF,[23] HPF,[24] NEID[25]) PRV spectrometers.

The baseline KPF spectrometer design is shown in Figure 5. Light enters the core spectrometer following the fiber image reformatter, at the focal point of the primary collimator mirror (traditionally this would be the location of the spectrometer slit). The f/8 beam diverges past this point and then strikes the primary collimator mirror (an off-axis paraboloid). Upon reflection, the now collimated 200 mm diameter light beam travels to the echelle grating, located one primary collimator focal length away from the primary collimator. After diffraction by the echelle, the diverging monochromatic beams reflect from the primary collimator a second time. Because the echelle grating is rotated slightly out of plane (the echelle gamma angle), the dispersed light does not return along the same path, and the pre- and post-diffraction beams are separated. Therefore, after reflecting from the collimator the second time, the dispersed light does not return to the entrance slit, but forms an intermediate focus to the side of the echelle. Just before the intermediate focus, a flat mirror is employed to fold the beam, to make the spectrometer footprint more compact.

After the fold mirror reflection, the light rays go through the intermediate focus, and then the diverging monochromatic beams are collimated by the secondary collimator mirror (an off-axis paraboloid). The monochromatic beam diameter here is 160 mm, owing to the secondary collimator having a focal length 0.8× that of the primary collimator. The converging monochromatic beams next encounter a dichroic beamsplitter, where wavelengths blueward of 593 nm are reflected, and wavelengths redward of 593 nm are transmitted. After reflection, the green channel monochromatic beams continue to converge towards the white pupil, where the cross-dispersion grism (grating prism) is located. This disperser consists of a shallow apex angle prism bonded to a volume phase holographic (VPH) grating. Following the grism, the light enters the camera, which then focuses the spectrum onto the CCD detector. A summary of various spectrometer parameters is given in Table 1, at the end of this section.

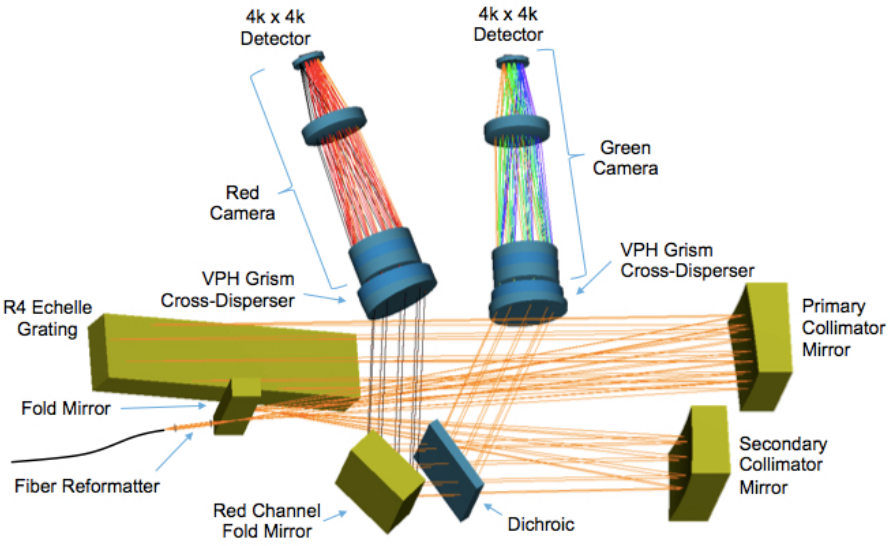

Figure 5. Optical layout of the KPF spectrometer.

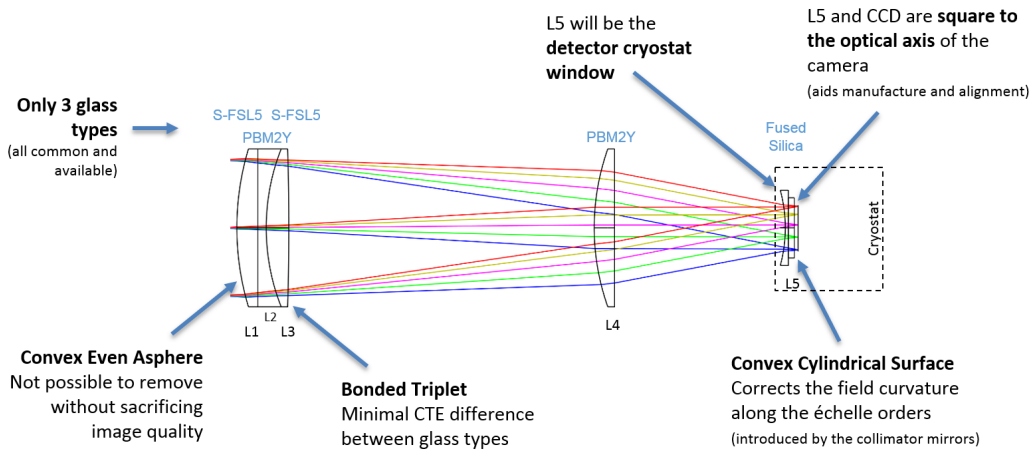

Figure 6. The baseline green channel camera design, with design highlights indicated. This meridional view is in the cross-dispersion direction, with the blaze wavelengths of five echelle orders shown. The L5 singlet lens doubles as the vacuum window for the detector, and has a stepped flange to accommodate an O-ring.

The asymmetry factor of 0.8 was chosen through a trade study exploring instrument size, camera aperture, camera focal length and camera field of view, VPH efficiency envelope and VPH line density. This value allows camera lenses under 250 mm in diameter (reduced camera cost), and compared to more aggressive asymmetry ratios allows a smaller camera field of view (less complicated camera design), and lower VPH line densities (broader VPH efficiency envelopes).

Employing a 200 mm collimated beam diameter with an R4 echelle grating leads to a grating 824 mm long, which forces a mosaic grating due to grating manufacturing constraints. We decided to use a mosaic with a monolithic substrate, as it was the option offering the highest mechanical stability (as opposed to a mechanical mosaic assembly employing two separate gratings).

The KPF cross-dispersion grism design follows the ESPRESSO[22] concept, although after a trade study we chose a less aggressive angle of incidence on the prism entrance face (30° instead of 50°). We have also adopted the ESPRESSO concept (ibid) of maximizing efficiency by using the VPH off the Bragg angle (with the angle of diffraction at zero for the central wavelength).

The KPF green channel camera optical layout is shown in Figure 6. The red camera is still in development, although we expect its design to be very similar to the green camera design. Both cameras will be five element Petzval designs, containing three groups of lenses. The design consists of a bonded triplet, followed by a singlet lens, and finally a field flattener just before the CCD detector. The first surface of the triplet is a convex even asphere, and the final surface of the field flattener is a convex cylinder. The starting point for this baseline design was the DESI red camera,[26] which was then scaled and optimized for KPF.

Small, compact spots were a priority during optimization, to help reduce the effect of pupil illumination changes on radial velocity precision (small spot sizes cannot have strong centroid shift reactions to pupil illumination changes, as the resulting centroid shift must always be less than the size of the spot). Uniform spots across an order were also emphasized during optimization, to mitigate point spread function (PSF) differences experienced by absorption lines as they change spectral position between observations owing to the barycentric Doppler shift.

After an in-house design effort, the camera design was sent to Winlight Systems for a review on performance, risk, manufacturability, potential improvements, ghosting, and costing. Their review was favorable, and notably they suggested changes in glass types, which maintained the image quality of the original design but lead to an improvement in throughput. The optimized Winlight Systems camera design (Figure 6) was then adopted as our baseline.

The KPF detectors will be 4k x 4k CCDs, with 15 μm pixels. The detector and cryostat systems will be designed, assembled, and tested by the University of California Observatories (UCO) for the KPF project. Initial

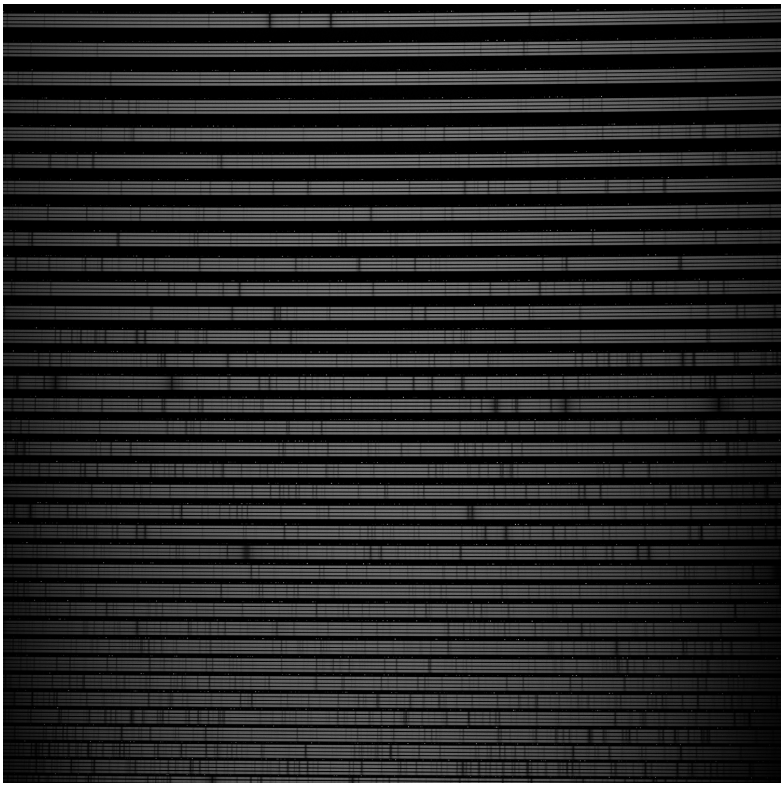

Figure 7. A Zemax-generated synthetic KPF spectrum. A solar spectrum was used for the three science slices and the sky fiber, and a Thorium-Argon spectrum was used for the simultaneous calibration fiber.

trade studies will be undertaken to determine the optimal green and red CCD choices, as well as the optimal cooling system, electronics, and detector mounting arrangement given KPF's high degree of required stability. Known detector-specific issues to be characterized and mitigated include vibration from the cooling system, CCD lithography errors, and detector heat output. The final point is an important one as the detectors will be the only sources of heat within the KPF spectrometer vacuum chamber.

Figure 7 shows a synthetic KPF spectrum, generated within Zemax.[27] The figure shows the five "orderlets" within each echelle order: simultaneous calibration, 3x science slices, and sky. Within the figure, a solar spectrum was used for the three science slices and the sky fiber, and a Thorium-Argon spectrum was used for the simultaneous calibration fiber.

3.5 Calibration System

The KPF calibration system will reside in the observatory basement near the spectrometer. This will consist of the typical spectrometer calibration sources (Thorium-Argon lamps for wavelength calibration and a quartz lamp for flat-fielding). Our conceptual design includes these sources feeding an integrating sphere (flux levels allowing), which will then feed two calibration fibers.

One fiber will travel up to the telescope, where the FIU will focus the calibration light onto the science and sky fibers (for calibrations between science exposures). The second fiber will travel directly to the spectrometer, to provide a simultaneous calibration source during a science exposure.

Within the integrating sphere will be a rotating mirror to mitigate modal noise effects within the calibration fibers (following the approach of Reference 28). Spare ports on the integrating sphere will easily allow a future upgrade to a high line density calibrant, such as a Fabry-Perot etalon or a laser frequency comb.

Table 1. KPF parameters summary table.

Parameter	**Value**
Optical design family	Asymmetric white pupil
Collimated beam diameter	200 mm
Collimator f/number	8
Asymmetric ratio	0.8
Resolving power	$>80{,}000$
Resolution element sampling (echelle dispersion)	3-4 pixels
Fiber details	Science: 250 μm octagonal Sky 250 μm octagonal Simultaneous calibration: 50 μm circular
Primary disperser	R4 echelle mosaic (Richardson MR263) 31.6 grooves per mm Substrate: 840 mm x 214 mm x 125 mm
Wavelength coverage	Green channel: 440 nm to 590 nm Red channel: 590 nm to 850 nm
Cross-dispersers	VPH grisms Green VPH: 810 lines per mm Red VPH: 450 lines per mm
Green Camera	Focal Length: 495 mm, f/2.9 Largest aperture: 210 mm diameter
Red Camera	Focal Length: 495 mm, f/2.9 Largest aperture: 240 mm diameter
Detector (Green and Red channels)	4k x 4k, 15 μm pixels

3.6 Calcium H & K Spectrometer

A separate small spectrometer will be used to monitor the Ca H & K lines for stellar activity that could mimic Doppler shifts. A major advantage of this approach is that the KPF spectrometer does not need to cover an increased bandpass blueward to 390 nm, and can stop at 443 nm (the Doppler information is reduced for G and K stars at bluer wavelengths owing to the significantly lower flux). This approach has important advantages with respect to optical coating bandpasses and efficiency, as well as the required detector size.

The Calcium H & K spectrometer will be a simple system (VPH-based with doublet lenses for collimator and camera), and be fiber fed via a UV-enhanced fiber (such as CeramOptec UVNS). Light will be injected into this fiber by the FIU, to capture this light before major UV absorption losses occur within the long fiber run.

3.7 Exposure Meter

An exposure meter will be employed to monitor the flux-weighted midpoint of each spectrum, required to accurately determine the barycentric correction and account for the movement of the Earth during the observation.

The KPF reformatter will reflect the smaller, outboard slices (shown in red at the left of Figure 3), to a lens which will focus the light into a fiber. This fiber will then travel though a feedthrough mounted on the vacuum chamber wall, and then through both walls of the thermal enclosure. With this approach, the heat source of the exposure meter detector is completely removed from within the spectrometer thermal enclosure.

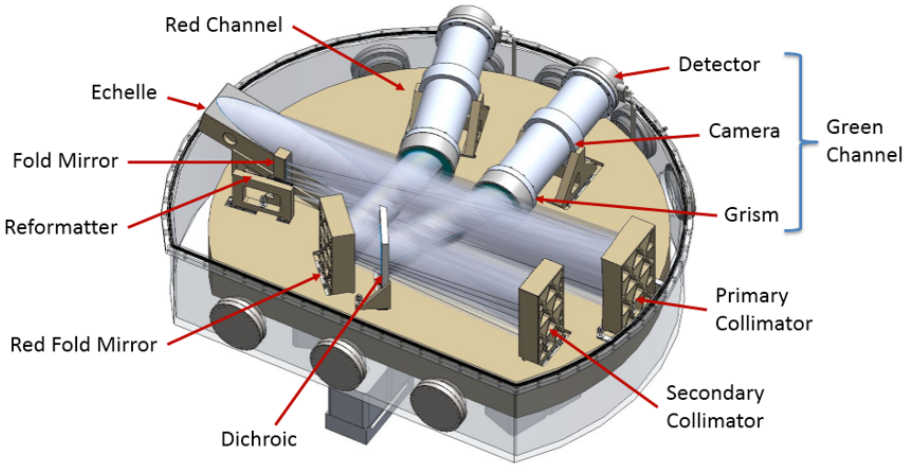

Figure 8. The KPF opto-mechanical concept, with the optical elements supported by a Zerodur bench. The lower section of the vacuum chamber is shown transparent for clarity.

4. OPTO-MECHANICAL DESIGN

In order to measure sub-m s^{-1} Doppler shifts, it is critical for a PRV spectrometer to have high mechanical stability. This section will outline the KPF opto-mechanical conceptual design.

4.1 Optical Bench and Optical Mounts

Stability analyses undertaken within Zemax have demonstrated that nanometer-level movements of the KPF optics cause spectral shifts at the m s^{-1} level.[29] Within PRV spectrometers such movements are typically constrained by exquisite, milli-Kelvin temperature control to minimize expansion and contraction effects (for example, HARPS[19] and HPF[30]). Within KPF, to minimize these effects we also intend to place the spectrometer within a thermal enclosure for temperature stability (at a level yet to be determined), while also utilizing low coefficient of thermal expansion (CTE) materials throughout the spectrometer. Minimizing local optic movements that shift the beam vertically with respect to the table is especially critical, as this is along the direction of echelle dispersion within the KPF design.

A unique aspect of KPF is the use of a Zerodur optical bench to support the spectrometer, as shown in Figure 8. Our bench source is a 2 m diameter by 0.4 m thick disk of Zerodur that was purchased for, (but then not utilized by), a previous SSL project (Figure 9, left).

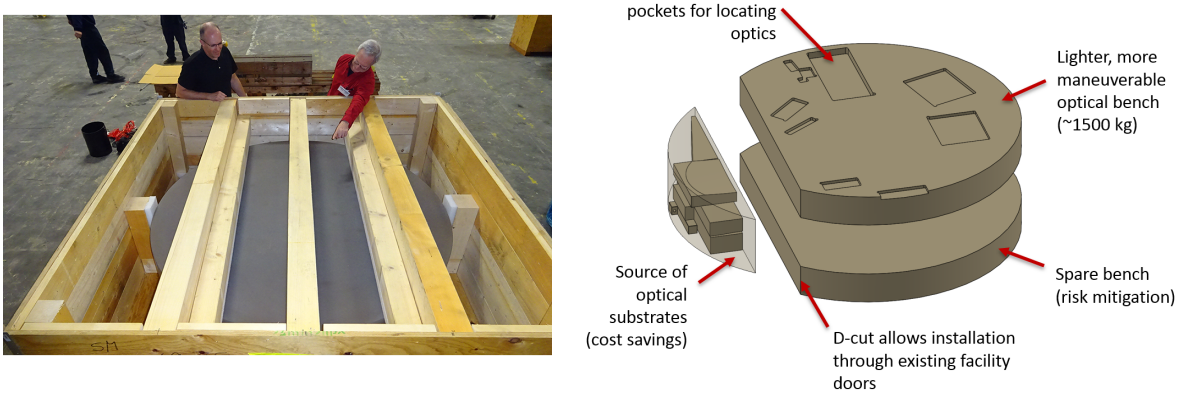

Figure 9. Left: Current view of the Zerodur disk, within its shipping crate. Right: Planned modifications to the Zerodur disk.

The primary advantage of a Zerodur bench is its small CTE value, and our particular disk has an extremely low CTE value (approximately 0.000 ± 0.004 x 10^{-6} K^{-1}, as measured by Schott). This CTE value is orders of magnitude smaller than metals typically used in optical benches. A further advantage is that Zerodur is an effective thermal insulator, and as such will resist thermal gradient propagation.

We intend to take full advantage of the low CTE bench by mechanically contacting optics and mounts - also made of Zerodur, where possible - directly to the Zerodur bench. We are specifically avoiding high CTE materials which are commonly used to mount optics (i.e. metals, RTV, plastics and epoxies). As such, we expect the KPF spectrometer to have a very high level of mechanical and thermal stability. A full structural-thermal-optical (STOP) model will be developed during the current preliminary design phase to verify this (and also to determine the temperature stability performance required of the thermal enclosure).

The full Zerodur disk must be modified as it weighs 3177 kg and will not fit through the door to the observatory basement. Therefore, we intend to cut the disk as shown in the right side of Figure 9. Also shown in the figure is our plan to utilize an un-used portion of the disk as the source for optical substrates.

Our baseline design is to CNC-machine pockets into the top surface of the optical bench, as shown on the right side of Figure 9. We have discussed this approach with Schott and found that their machining tolerances are adequate to meet our optical alignment tolerances. Two intersecting walls within each pocket are used as reference surfaces to locate an optical element sitting within the pocket.

During assembly, an optic will be placed into a pocket, and then pushed into the corner between the two pocket reference edges. As shown in Figure 10, each optic will have three feet on the bottom, to rest on the pocket floor, and three pads on the sides of the optic, to contact the reference walls of the pockets. The feet and side pads will be machined directly into the substrates, and then re-machined or hand-lapped if necessary to ensure the alignment tolerances between the pads and the optical axis are met. We have discussed this technique with two vendors and both have ensured its feasibility. We intend to investigate the alignment precision and repeatability, and stability of this technique with a prototype mount during the preliminary design phase.

Once placed with the reference pads in contact with the bench pockets, the optic will then be held in this location by spring force. With this method, the Zerodur optic (or mount) is in direct contact with the Zerodur bench, and the expansion and contraction of the springs cannot influence the position of the optic (rather only slightly affect the spring force they apply to the optic). As shown in Figure 10, three springs are required for each optic: one vertical spring (to provide downward force against the pocket floor), and two horizontal springs (to provide sideways force against the pocket reference walls).

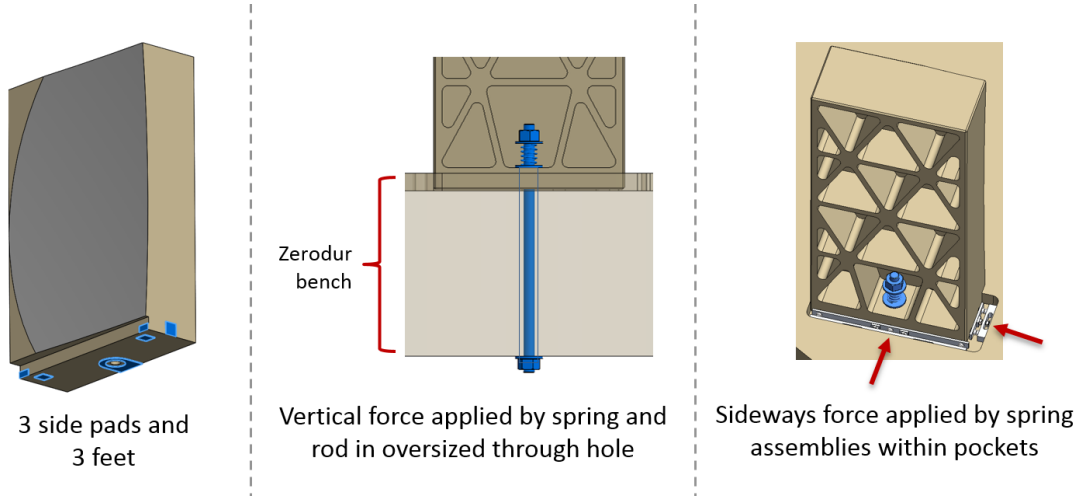

Figure 10. Left: Each optic will have integral mounting features. Middle, Right: Springs will be used to hold the optics to the bench and maintain the Zerodur-to-Zerodur contact.

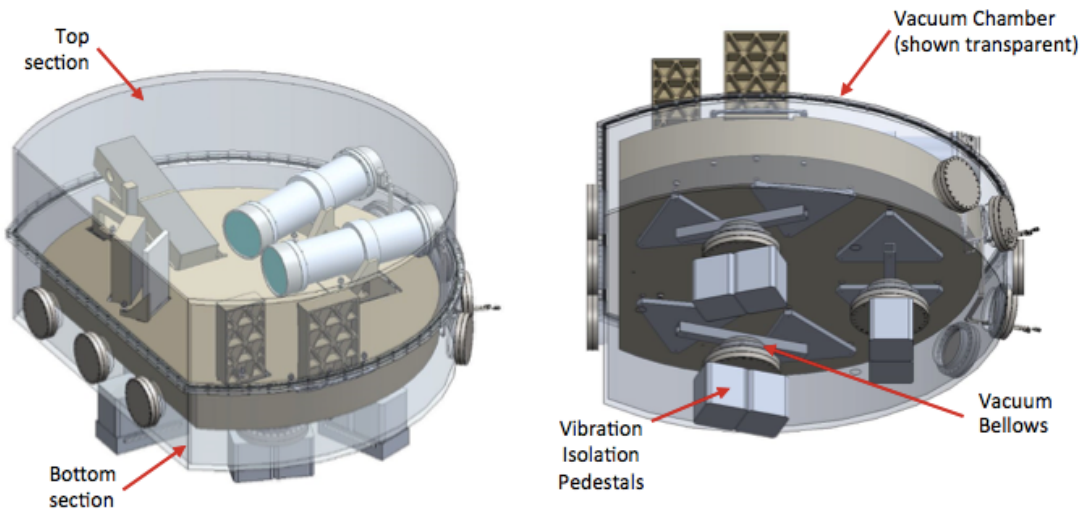

Figure 11. Left: The KPF vacuum chamber. Right: Zerodur bench support concept.

4.2 Vacuum Chamber and Optical Bench Support

In order to isolate the spectrometer from its environment, it will be placed within a vacuum chamber (for isolation against changes in atmospheric pressure), and also within a pair of nested, insulated rooms (for isolation against temperature changes at the milli-Kelvin level, which can affect the spectrometer through expansion and contraction).

The baseline KPF vacuum chamber is shown at the left of Figure 11; the overall dimensions of the system shown are 1500 mm x 2400 mm x 2400 mm. The chamber is made up two sections, with each section sized to fit through the double doors into the observatory, and also to allow assembly given the basement ceiling height. We are investigating adding ribs to the top and flat chamber sides to increase strength and minimize chamber wall thickness and weight.

As shown in Figure 11, the chamber will have several ports for gauges, valves, and feedthroughs. All ports will be located on the lower section of the chamber, allowing the chamber lid to be removed without disconnecting any of the various fibers, cables and hoses passing through the vacuum chamber walls. This approach means the spectrometer remains operational with the chamber lid removed (desirable for integration and testing).

The KPF optical bench will be supported by an 18-point whiffletree support system, as shown at the right of Figure 11. Six triangles, with three points each in contact with the bench, are distributed around the bottom of the Zerodur bench. A pair of triangles is then supported by a bar, which is then connected to a vibration isolator pedestal through a vacuum bellow. The flexible vacuum bellows will ensure that tank flexure due to atmospheric pressure changes does not transmit into the whiffletree structure and affect the stability of the optical bench. The vibration isolator serves to isolate the optical bench from floor vibrations (which we have measured within the beam combining room).

The whiffletree will not be a rigid structure, but will have flexible joints where the triangles meet the bars, and where the bars meet the isolation supports. This allows the whiffletree to support the bench, yet still be flexible enough to not induce stress into the Zerodur disk.

5. PERFORMANCE METRICS

Two performance metrics are being tracked throughout the development process: a Doppler stability budget and a system throughput estimation.

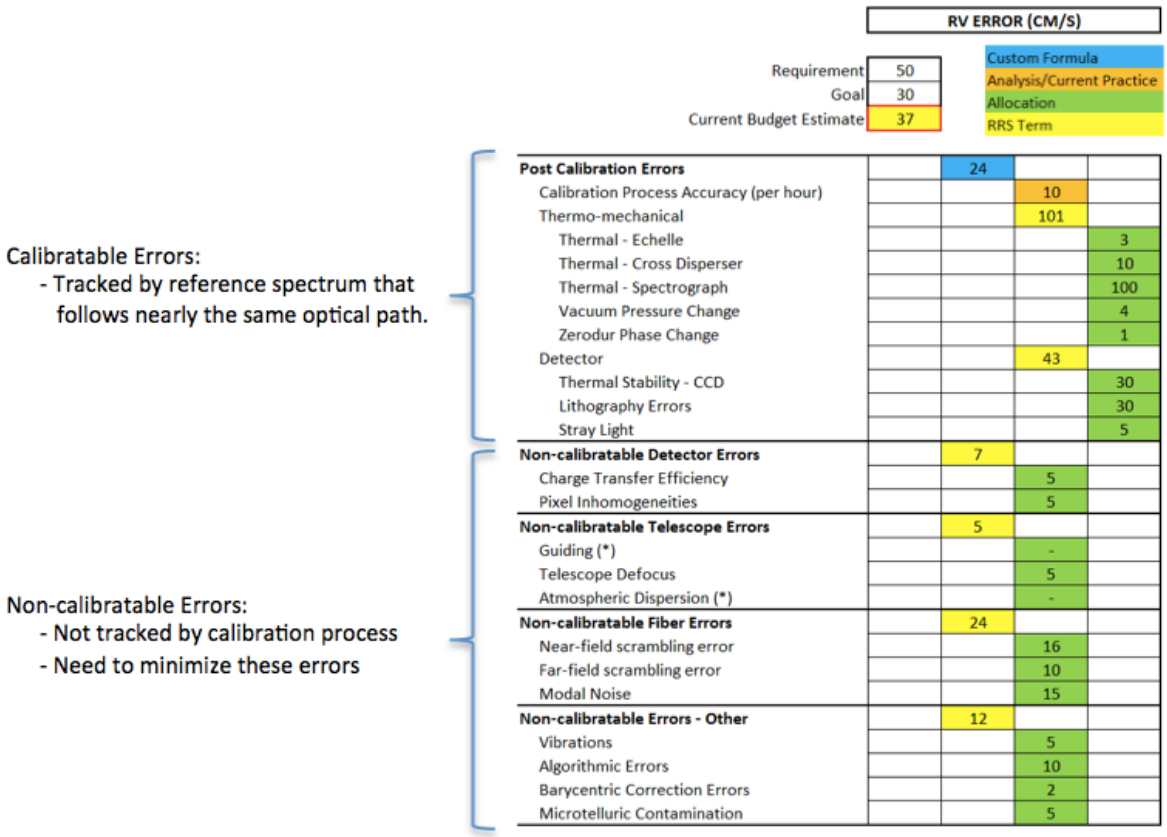

Figure 12. Initial KPF Doppler stability budget.

5.1 Doppler Stability

The KPF Dopper stability budget is presented in Figure 12. This stability budget format is based on the G-CLEF format, as presented in Reference 31. It is a Root Sum Squared (RSS) approach, and as shown in Figure 12 is composed of two main parameter groups: errors that can be tracked by calibration methods (and minimized), and errors that cannot be removed or minimized by calibration. It is assumed that for the calibratable errors, 90% of the error can be removed through appropriate calibrant tracking (meaning only 10% of these errors remain in the final data).

The values within this table will be updated as development proceeds. For example, the thermal effects will be better understood after the STOP analysis of our spectrometer system. We aim to characterize the CCD-specific errors, through direct measurement of our CCD sensors on a test bench, before integration within the spectrometer. The contributions of the fiber errors will be better understood through the continued testing of our fiber homogenization system in the laboratory. Finally, the algorithmic errors will be monitored closely during the development of the KPF data analysis pipeline.

5.2 Throughput Estimate

The preliminary green channel spectral efficiency profile is shown in Figure 13, including all elements from the top of the telescope to the spectrometer CCD. As shown in the figure, the peak efficiency of the system is 8.5% at 551 nm. The efficiency is lower at the blue end of the wavelength range. While this is typical for optical instruments, within KPF it is especially driven by the 70 m fiber path. The equivalent red channel spectral efficiency estimation (and also the impact of the dichroic) are currently under development. We expect the red channel spectral efficiency curve to be more uniform, as it will not suffer the blue-specific losses incurred by the fiber system.

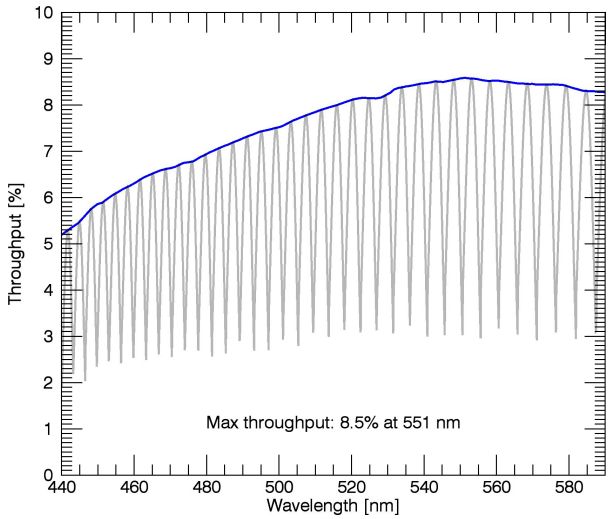

Figure 13. The KPF predicted throughput across the green channel bandpass, from the top of the telescope to the spectrometer CCD. Shown in grey are the intensity profiles of the individual echelle diffraction orders, each over one free spectral range. For clarity, the blue curve connects the order blaze peaks.

Figure 14 shows the predicted efficiency losses contributed by each surface that the light encounters between the top of the telescope and the spectrograph CCD. Three wavelengths are shown, indicating the center, and blue and red extremes of the KPF green channel wavelength coverage.

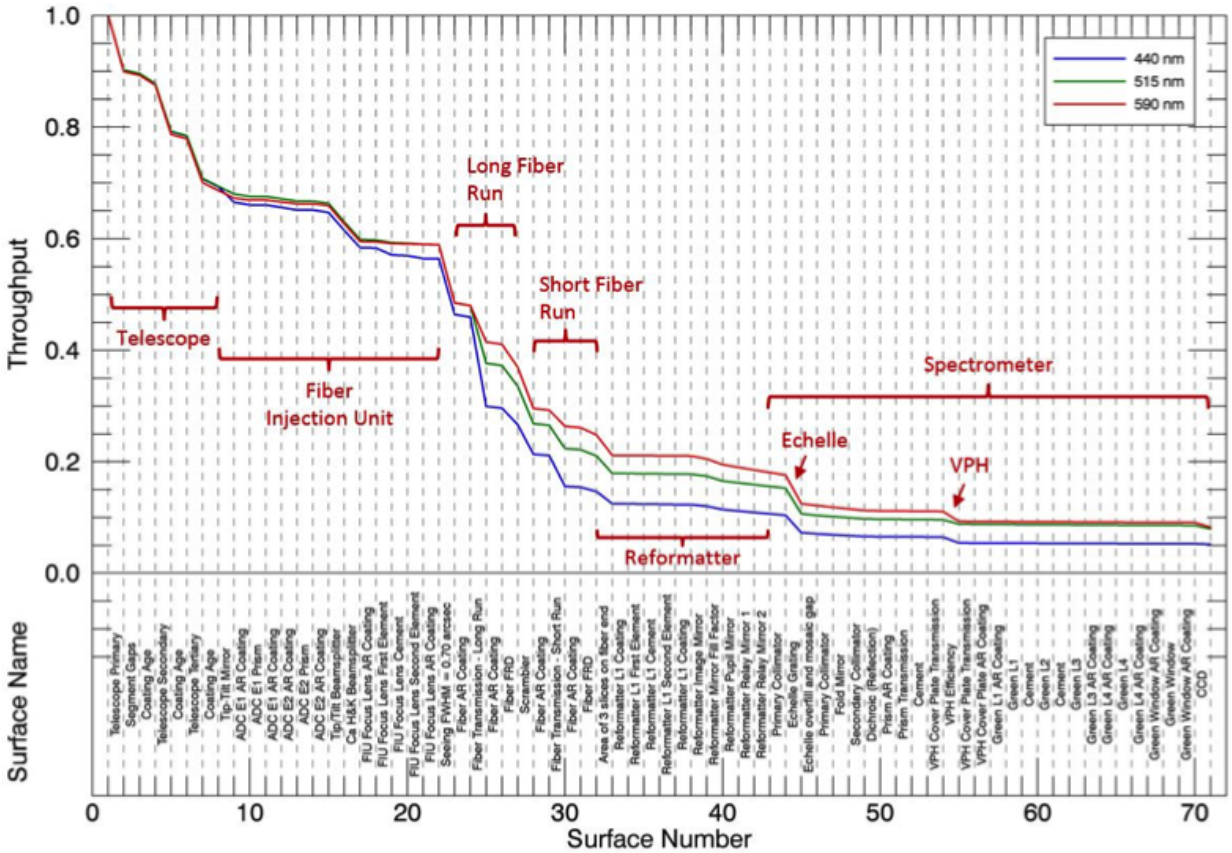

Figure 14. Green channel surface-by-surface losses as light travels through the KPF system from the top of the telescope to the spectrometer CCD.

ACKNOWLEDGMENTS

The authors thank the W.M. Keck Foundation, the Heising-Simons Foundation, the University of California, Berkeley, and the University of Hawai'i for financial support of KPF. The authors also wish to thank the technical and engineering staff at the W.M. Keck Observatory (in particular Sean Adkins), as well as Connie Rockosi, David Cowley, and Dale Sandford of the University of California Observatories detector group. The contributions of Daniel Finstad, Yuzo Ishikawa, Tim Miller, Jeremy McCauley and Christopher Smith of the Space Sciences Laboratory are also noted, along with Trish Dobson and the Lab's administrative support team.

REFERENCES

[1] Howard, A. W. et al., "The Occurrence and Mass Distribution of Close-in Super-Earths, Neptunes, and Jupiters," *Science* **330**, 653 (Oct. 2010).

[2] Mayor, M. et al., "The HARPS search for southern extra-solar planets XXXIV. Occurrence, mass distribution and orbital properties of super-Earths and Neptune-mass planets," *arXiv:1109.2497* (Sept. 2011).

[3] Petigura, E. A., Howard, A. W., and Marcy, G. W., "Prevalence of Earth-size planets orbiting Sun-like stars," *Proceedings of the National Academy of Science* **110**, 19273–19278 (Nov. 2013).

[4] Howard, A. W. et al., "Planet Occurrence within 0.25 AU of Solar-type Stars from Kepler," *ApJ* **201**, 15 (Aug. 2012).

[5] Sullivan, P. W. et al., "The Transiting Exoplanet Survey Satellite: Simulations of Planet Detections and Astrophysical False Positives," *ApJ* **809**, 77 (Aug. 2015).

[6] Adkins, S. M. et al., "MAGIQ at the W. M. Keck Observatory: initial deployment of a new acquisition, guiding, and image quality monitoring system," in [*Ground-based and Airborne Instrumentation for Astronomy II*], *Proc. SPIE* **7014**, 70141U (July 2008).

[7] Queloz, D., Casse, M., and Mayor, M., "The Fiber-Fed Spectrograph, a Tool to Detect Planets," in [*IAU Colloq. 170: Precise Stellar Radial Velocities*], Hearnshaw, J. B. and Scarfe, C. D., eds., *Astronomical Society of the Pacific Conference Series* **185**, 13 (1999).

[8] Perruchot, S. et al., "Higher-precision radial velocity measurements with the SOPHIE spectrograph using octagonal-section fibers," *Proc. SPIE* **8151** (Sept. 2011).

[9] Avila, G., "FRD and scrambling properties of recent non-circular fibres," in [*Ground-based and Airborne Instrumentation for Astronomy IV*], *Proc. SPIE* **8446**, 84469L (Sept. 2012).

[10] Hunter, T. R. and Ramsey, L. W., "Scrambling properties of optical fibers and the performance of a double scrambler," *PASP* **104**, 1244–1251 (Dec. 1992).

[11] Halverson, S. et al., "An Efficient, Compact, and Versatile Fiber Double Scrambler for High Precision Radial Velocity Instruments," *ApJ* **806**, 61 (June 2015).

[12] Avila, G. et al., "Performances of HARPS and FEROS fibers in La Silla ESO Observatory," in [*Ground-based Instrumentation for Astronomy*], Moorwood, A. F. M. and Iye, M., eds., *Proc. SPIE* **5492**, 669–676 (Sept. 2004).

[13] McCoy, K. S. et al., "Optical fiber modal noise in the 0.8 to 1.5 micron region and implications for near infrared precision radial velocity measurements," in [*Ground-based and Airborne Instrumentation for Astronomy IV*], *Proc. SPIE* **8446**, 84468J (Sept. 2012).

[14] Plavchan, P. P. et al., "Precision near-infrared radial velocity instrumentation II: noncircular core fiber scrambler," in [*Techniques and Instrumentation for Detection of Exoplanets VI*], *Proc. SPIE* **8864**, 88640G (Sept. 2013).

[15] Roy, A., Halverson, S., Mahadevan, S., and Ramsey, L. W., "Scrambling and modal noise mitigation in the Habitable Zone Planet Finder fiber feed," in [*Ground-based and Airborne Instrumentation for Astronomy V*], *Proc. SPIE* **9147**, 91476B (July 2014).

[16] Finstad, D. et al., "Scrambling gain of non-circular core fibers being tested for use in the Keck Planet Finder instrument," in [*Ground-based and Airborne Instrumentation for Astronomy VI*], *Proc. SPIE* **9908**, 9908283 (June 2016).

[17] Vivès, S., Prieto, E., and Madec, F., "A set of Zemax user-defined surfaces to model slicer mirrors," *Proc. SPIE* **6273**, 62731R (June 2006).

[18] Vivès, S. et al., "New technological developments in integral field spectroscopy," in [*Advanced Optical and Mechanical Technologies in Telescopes and Instrumentation*], *Proc. SPIE* **7018**, 70182N (July 2008).
[19] Mayor, M. et al., "Setting New Standards with HARPS," *The Messenger* **114**, 20–24 (Dec. 2003).
[20] Cosentino, R. et al., "Harps-N: the new planet hunter at TNG," **8446** (Sept. 2012).
[21] Quirrenbach, A. et al., "CARMENES instrument overview," in [*Ground-based and Airborne Instrumentation for Astronomy V*], *Proc. SPIE* **9147**, 91471F (July 2014).
[22] Spanò, P. et al., "Very high-resolution spectroscopy: the ESPRESSO optical design," in [*Ground-based and Airborne Instrumentation for Astronomy IV*], *Proc. SPIE* **8446**, 84467V (Sept. 2012).
[23] Szentgyorgyi, A. et al., "A preliminary design for the GMT-Consortium Large Earth Finder (G-CLEF)," in [*Ground-based and Airborne Instrumentation for Astronomy V*], *Proc. SPIE* **9147**, 914726 (Aug. 2014).
[24] Mahadevan, S. et al., "The Habitable-zone Planet Finder: A status update on the development of a stabilized fiber-fed near-infrared spectrograph for the for the Hobby-Eberly telescope," in [*Ground-based and Airborne Instrumentation for Astronomy V*], *Proc. SPIE* **9147**, 91471G (July 2014).
[25] Schwab, C., "Optical design for NEID, a proposed spectrometer for NASA's WIYN extreme precision Doppler spectrometer," in [*Ground-based and Airborne Instrumentation for Astronomy VI*], *Proc. SPIE* **9908** (June 2016).
[26] Jelinsky, P. et al., "The BigBOSS spectrograph," in [*Ground-based and Airborne Instrumentation for Astronomy IV*], *Proc. SPIE* **8446**, 844668 (Sept. 2012).
[27] Gibson, S. R. and Wishnow, E. H., "A method for generating a synthetic spectrum within Zemax," in [*Systems Engineering V: Tools and Processes*], *Proc. SPIE* **9911** (June 2016).
[28] Halverson, S. et al., "The habitable-zone planet finder calibration system," in [*Ground-based and Airborne Instrumentation for Astronomy V*], *Proc. SPIE* **9147**, 91477Z (Aug. 2014).
[29] Gibson, S. R., "Tolerancing a radial velocity spectrometer within Zemax," in [*Systems Engineering V: Tools and Processes*], *Proc. SPIE* **9911**, 991190 (June 2016).
[30] Hearty, F. et al., "Environmental control system for Habitable-zone Planet Finder (HPF)," in [*Ground-based and Airborne Instrumentation for Astronomy V*], *Proc. SPIE* **9147**, 914752 (July 2014).
[31] Podgorski, W. et al., "A novel systems engineering approach to the design of a precision radial velocity spectrograph: the GMT-Consortium Large Earth Finder (G-CLEF)," in [*Ground-based and Airborne Instrumentation for Astronomy V*], *Proc. SPIE* **9147**, 91478W (July 2014).